Metal Enhanced Fluorescence on Super-Hydrophobic Clusters of Gold Nanoparticles

Edmondo Battista, Maria Laura Coluccio, Alessandro Alabastri, Marianna Barberio, Filippo Causa, Paolo Antonio Netti, Enzo Di Fabrizio, Francesco Gentile

PII: S0167-9317(16)30518-4
DOI: doi:10.1016/j.mee.2016.12.013
Reference: MEE 10408

To appear in:

Received date: 13 October 2016
Revised date: 12 December 2016
Accepted date: 14 December 2016

Please cite this article as: Edmondo Battista, Maria Laura Coluccio, Alessandro Alabastri, Marianna Barberio, Filippo Causa, Paolo Antonio Netti, Enzo Di Fabrizio, Francesco Gentile, Metal Enhanced Fluorescence on Super-Hydrophobic Clusters of Gold Nanoparticles, (2016), doi:10.1016/j.mee.2016.12.013

Metal Enhanced Fluorescence on Super-Hydrophobic Clusters of Gold Nanoparticles

Edmondo Battista[a,b]*, Maria Laura Coluccio[c], Alessandro Alabastri[d], Marianna Barberio[e], Filippo Causa[a,b], Paolo Antonio Netti[a,b], Enzo Di Fabrizio[c,f], Francesco Gentile[g]

[a]Interdisciplinary Research Center on Biomaterials and DICMAPI, University Federico II, P.le Tecchio 80, Naples, Italy

[b]Center for Advanced Biomaterials for HealthCare @CRIB, Istituto Italiano di Tecnologia, Largo Barsanti e Matteucci 53, Naples, Italy

[c]Department of Experimental and Clinical Medicine, University of Magna Graecia, 88100 Catanzaro, Italy

[d]Physics and Astronomy Department, Rice University, Houston, Tx, USA

[e]Ipat-lab, INRS-EMT, 1650 Boul Lionel Boulet, Varennes (Qb), Canada

[f]PSE division, King Abdullah University of Science and Technology, Thuwal 23955 − 6900, Saudi Arabia

[g]Department of Electrical Engineering and Information Technology, University Federico II, Naples, Italy

*corresponding author: edmondo.battista@unina.it

We used optical lithography, electroless deposition and deep reactive ion etching techniques to realize arrays of super-hydrophobic gold nanoparticles arranged in a hierarchical structure. At the micro-scale, silicon-micro pillars in the chip permit to manipulate and concentrate biological solutions, at the nano-scale, gold nanoparticles enable metal enhanced fluorescence (MEF) effects, whereby fluorescence signal of fluorophores in close proximity to a rough metal surface is amplified by orders of magnitude. Here, we demonstrated the device in the analysis of fluorescein derived gold-binding peptides (GBP-FITC). While super-hydrophobic schemes and MEF effects have been heretofore used in isolation, their integration in a platform may advance the current state of fluorescence-based sensing technology in medical diagnostics and biotechnology. This scheme may be employed in protein microarrays where the increased sensitivity of the device may enable the early detection of cancer biomarkers or other proteins of biomedical interest.

Keywords: Metal Enhanced Fluorescence (MEF), Super-Hydrophobic Surfaces, Gold Nanoparticles, Electroless Deposition, Gold-binding Peptides, Fluorescence Lifetime Microscopy (FLIM)

1 Introduction

The new paradigm of Materials Science is realizing materials in which the structure of the material itself is controlled at a molecular level [1]. Similar nano-scale materials display enhanced properties with respect to their macro-scale counterparts. Excellent properties associated with nanostructures of controlled geometry has opened up exciting opportunities for

new materials design and will potentially revolutionize current practice in biology and medicine. Metal enhanced fluorescence (MEF) is a physical effect that occurs when fluorophores are located in close proximity to a rough metal surface [2-5]. In MEF, silver or gold nanoparticles with a regular rather than periodic motif interact with an electromagnetic field to yield site specific increments of that field. This in turn allows to obtain the fluorescence signature of biological molecules with unprecedented sensitivity and thus to diagnose a disease at the very early stages of its progression. Compared to conventional fluorescence, MEF benefits of increased spontaneous emission rate, quantum yield and photo-stability, decreased fluorescent lifetime of fluorophores, directional emission [3]. In MEF, fluorescence amplification depends on three separate mechanisms, that are, (i) energy transfer from the fluorophore to the metal; (ii) enhancement of the local electromagnetic field; (iii) modification of the radiative decay rate of the fluorophore through the local modification of the photon density of states [3]. Mechanisms from (i) to (iii) are driven by the geometry of the metal/fluorophore interface. Designing and fabricating such interface at the submicron or nanoscale dimension, and controlling its nano-topography, may lead to MEF devices with enhanced sensitivity, reliability, signal to noise ratio. Here, we used optical lithography, Reactive Ion Etching and electroless deposition [6, 7] techniques to obtain super-hydrophobic silicon micro-pillars (**Figure 1a**), where the surface of the pillars is decorated with gold nanoparticle clusters (**Figure 1b-c**). The device incorporates multiple functionalities that arise because of the multiscale/hierarchical structure of the material. At the micro-meter dimension, silicon micro-pillars manipulate and concentrate diluted solutions as precedently described in [8, 9], at the nano-meter dimension, gold nano-grains modify locally the electromagnetic field (**Figure 2**) to generate enhanced MEF signals. To demonstrate the device, we selectively adsorbed a fluorescein derived GBP-FITC peptide onto the gold nanoparticles; then we verified peptide/metal binding and resulting enhancement of fluorescence through fluorescence microscopy and fluorescence lifetime microscopy (**Figure 3**). This technology may be employed in protein microarrays where the increased sensitivity of the device may enable the detection of cancer biomarkers or other proteins of biomedical interest in heretofore unattainable detection ranges.

2 Methods

2.1 Fabrication of the device. We used P type (100) Silicon wafers as substrates. After cleaning with acetone, substrates were spin-coated with a S1813 positive tone resist (from Rohm and Haas). Standard optical lithography techniques (Karl Suss Mask Aligner MA 45, Suss MicroTec GA, Garching, Germany) were used to generate patterns of holes in the resist, with an average diameter $d = 10\ \mu m$ and pattern to pattern distance $\delta = 20\ \mu m$. The diameter to gap 1: 2 ratio guaranties the best compromise between non-wettability and long evaporation times of a solution in a non-wetting/Cassie state [10]. Gold nanoparticles were deposited in the holes using electroless deposition techniques as described in references [6, 7] and recapitulated below. The residual resist was removed with acetone and the sample was processed with Bosch Reactive Ion Etching (MESC Multiplex ICP, STS, Imperial Park, Newport, UK) to generate patterns of cylindrical pillars where the height of the pillars is $h = 15\ \mu m$. Electroless grown Au particles served as a mask during the reactive ion etching (RIE) process. The samples were finally covered with a thin (few nm) film of a Teflon-like (C4F8) polymer to assure hydrophobicity. The masks for optical lithography were fabricated using Electron Beam Lithography (Crestec CABL-9000C electron beam lithography system). The Bosch DRIE process is a pulsed, time-multiplexed etching that alternated repeatedly between three modes, namely (i) a deposition of a chemically inert passivation layer of C_4F_8; (ii) an isotropic plasma etch of SF_6; and (iii) a phase for sample/chamber cleaning. Based on this alternate process, the pillars were fabricated with nano-threads at the sidewalls. The ratio between the times of passivation and etching was adjusted with precision to ensure vertical sidewalls [11].

2.2 Electroless deposition of gold nanoparticles clusters. Electroless deposition is based on an autocatalytic chemical reduction of metal ions in an aqueous solution when silicon nanoparticles are present. Gold ions exchange electrons with the silicon substrate that is the reducing agents itself. The reaction occurs in a $0.15\ M$ solution of fluoridric acid (HF) solution containing the silicon substrate and auric chloride ($AuCl_3$). The gold salt concentration C and the process conditions: temperature T and reaction time t are adjusted as $C = 5\ mM, T = 50°C, t = 120\ s$. The driving force in this process is the difference between the redox potentials of the two half-reactions, gold reduction and silicon oxidation, which depends on solution temperature, concentration and pH, explaining the reason because these parameters influence the particles size and density. For this configuration, we have the following reactions, at the anode (that is, silicon oxidation):

$$Si + 2H_2O \rightarrow Si\,O_2 + 4\,H^+ + 4\,e^- \quad (1)$$

And at the cathode (that is, gold reduction)

$$Au^{3+} + 3\,e^- \rightarrow Au^0 \quad (2)$$

Where the standard potentials apply

$$E_{01} = -0.9\,V, \quad (3)$$

$$E_{02} = 1.52\,V.$$

2.3 SEM Characterization SEM images of the the pillars and the gold nanoparticles clusters were captured using a Dual Beam (SEM-FIB) - FEI Nova 600 NanoLab system. The beam energy and the corresponding electron current were maintained fixed as 15 keV and 0.14 nA throughout the acquisitions.

2.4 AFM characterization Atomic force microscopy (ICON) was used for sample characterization. All the measurements were performed in a dry environment in intermittent contact mode over a sampling area of $1 \times 1\ \mu m^2$. Room temperature was hold fixed for all the acquisitions. Ultra-sharp Si probes with a nominal tip radius less than $5\ nm$ were used for achieve high resolution. Multiple measurements were done in different scan directions to avoid artefacts. At least four images in height mode (trace and retrace) were recorded per sample. The images had a resolution of 512×512 points and were acquired at a scanning rate of $1\ Hz$. Processing the images with fast Fourier transform algorithms permitted to extract and decode their information content, and ultimately derive the fractal dimension of the substrates.

2.5 Deriving the fractal dimension of the samples The AFM profiles of the gold nanoparticles clusters were processed using the algorithms developed and described in references [12-14] , this permitted to derive for each image a characteristic power spectrum density function, which appears as a line with a slope β in a bi logarithm plot. β is related to the Hurst parameters as $\beta = 2(H + 1)$. The fractal dimension D_f of a surface can be derived from β as $D_f = (8 - \beta)/2$.

2.6 Surface Functionalization The device surface was treated by fluorescent $GBP - FITC$ (gold binding peptide fluorescein), made of a sequence previously selected by phage display to be selective for gold ($AuPi_3$: TLLVIRGLPGAC) [15-17] and at flanking region with the sequence $-$G4 $-$ RGDSPKC (FITC) (MW: 2469.82 Da, purchased from Proteogenix, France). Peptide was dissolved in HBS (10 mM Hepes, 150 mM N_aCl, 3 mM EDTA, pH 7.4) at the concentration of 30 µM. Gold surface was cleaned in a 5% (w/v) water solution of sodium hypochlorite for 5 min, then washed with ethanol (95 %) and dried with nitrogen. The molecular binding was

carried out by dropping 4 µl of solution on surfaces. The drop was left to adsorb for 30 min, rinsed with 3 ml HBS afterward and then dried with nitrogen.

2.7 Fluorescence microscopy Confocal fluorescence was recorded by means of a Leica inverted microscope SP5 from Leica Microsystems using a water immersion objective $25 \times$ (NA 0.95). To investigate the binding of GBP − FITC, the system was excited with an Ar^+ laser at 488 nm and the emission bandwidth was from 520 to 600 nm. All the images were collected at 12 bit color depth with a resolution of 1024×1024.

2.8 Fluorescence lifetime images (FLIM) of GBP − FITC adsorbing nanostructures were acquired by using a pulsed Multiphoton Laser source (120 fs, 80 MHz, Ultra, Chamaleon, Coherent, Santa Clara CA, US) implemented in the time-domain using a time-correlated single photon counting (TCSPC) module. The laser was tuned to 780 nm for two-photon excitation of fluorescein derivative by TCSPC, acquiring in the emission range 520-550 nm. Images and lifetime data were analyzed by using SymPhoTime software (PicoQuant, Germany) with the tail fitting methods adopting an iterative approach of exponential choice minimizing the error χ^2.

2.9 Simulating EM fields around NPs clusters Electromagnetic calculations on Au clusters were performed utilizing a commercial software (COMSOL v5.2) based on the Finite Element Method (FEM). Electromagnetic fields were calculated placing the nanoparticles on a PMMA substrate (refractive index nPMMA= 1.49). The substrate has length of 0.5 µm, width of 0.5 µm and thickness of 100 nm. The remaining background domain was considered to be air (nAIR= 1) and is 100 nm thick. Electric permittivities for Au were utilized according to Rakic et al. [18]. The simulation domain was truncated by using 10 nm thick Perfectly Matched Layers (PML) at the boundaries of the system. Free tetrahedral mesh elements with maximum size of $w_{max} = \lambda_{min}/5$ with $\lambda_{min} = 514\ nm$ were utilized. The source is a plane wave normally incident on the substrate. The cluster of nanoparticles is composed of partially overlapping spheres (**Figure 2a**) with diameters ranging from 50 to 60 nm. The centers of the spheres lie on the same plane and their volume is equally split between the PMMA substrate and the air domain.

3 Results

3.1 Super-Hydrophobic clusters of gold NPs The proposed top down/bottom up approach delivers the ability to produce super-hydrophobic clusters of gold nanoparticles with a tight

control over the physical characteristics of the system, including diameter and center to center distance of the silicon micro-pillars, and size and shape of the NPs which are integrated in the pillars. Several SEM images (**Figure 1**) were taken to assess sample uniformity and reproducibility. In **Figure 1a**, silicon micro-pillars are disposed on the substrate to reproduce an hexagonal lattice in which the diameter of the pillars is $d = 10$ μm and the pillar to pillar gap is $\delta = 20$ μm (the scale bar in the image is 40 μm). Higher magnifications as in **Figure 1b** (scale bar: 5 μm) and **c** (scale bar: 500 nm) reveal the topography of the upper surface of the pillar and the morphology of the gold NPs. Gold nanoparticles are quasi-spherical in shape with an average size of $S = 60\ nm$ and small deviations from the mean. Surface nano-topography of the samples (**Figure 1d**) was acquired using standard AFM. From the surface profile we derived a power spectrum PS (**Figure 1e**) that delivers the information content of the surface across different length-scales[12]. In a log-log diagram, the PS exhibits a linear behaviour with slope β in a region of the diagram. The smaller β, the longer the intervals over which the PS exhibits a constant value, that is, the information content of the system is maintained over multiple scales. Thus β is not independent from the fractal dimension D_f and from the measure of β one may obtain D_f as described in the methods. For the present configuration, the dimension of the nano-grains clusters reads as $D_f \sim 2.4$, that is strictly larger than the Euclidean dimension of a surface $D = 2$. Similar particle distributions in the plane manipulate incident electro-magnetic (EM) fields to yield enhancements of those fields up to 15-fold increases (**Figure 2b**). Recalling that the MEF effect depends on the square of the EM field around the intended structures [3-5], similar nano-geometries may yield amplifications of fluorescence up to 10^2 times. EM increments are calculated as the ratio between the EM field intensity measured on the device over the value of the intensity of the incident EM radiation. Moreover, Figure 2c indicates the simulated surface charge distribution in the nano-particles clusters reported in Coulomb.

3.2 Metal Enhanced Fluorescence on Super-Hydrophobic gold Nanoparticles The described devices were functionalized with a fluorescent $GBP - FITC$ gold binding peptide as described in the methods. **Figure 3b** shows the fluorescent profile measured over a pattern of super-hydrophobic gold nanoparticles clusters compared to a profile measured over bidimensional patterns of non-functionalized gold nano-particles (**a**). As formerly demonstrated by Causa and colleagues [16, 17] the $AuPi_3$ sequence, selected by phage display, is affine to gold surfaces with

which forms tight bonds. This explains the increased fluorescence signal on the super-hydrophobic gold nanoparticles as in **Figure 3b** in contrast to the vanishingly small signal emitted by the lattice of non-functionalized gold nano-particles (**a**). Cross section of gold nanoparticles clusters on the surface of an individual pillar as in **Figure 3c** reveals the spatial extension of the fluorescence intensity that stretches out in the longitudinal (axial symmetry of a pillar) direction to reach up to 1 μm below the upper surface of the pillar. The increased fluorescence emission efficiency of the devices is confirmed by the FLIM images as reported in **Figure 3d-e** for the (**d**) un-treated and the (**e**) clusters of super-hydrophobic gold nanoparticles where the peptide was adsorbed. The images show a different decay time in correspondence of the nanoclusters: the untreated surfaces show the characteristic two photon luminescence decay profile for nanostructured gold; while on the pillars, where the GBP-FITC is specifically adsorbed, we registered an average lifetime of 0.8 ns (see Table 1 for a detailed transcription of FLIM data). The decrease of fluorescence lifetime in correspondence of rough nanostructured gold is predicted by the MEF theory.

Moreover, another aspect for which super-hydrophobic rough metal nano-structures are preferable to conventional materials, is that MEF is correlated to an enhanced fluorophore photo-stability as the fluorophores stay less time in an excited state, before falling to their pristine ground state, and are therefore less susceptible to photo-destruction [2] [19]. Taken together, **Figures 3a-e** show significant fluorescence enhancements when fluorophores interact with rough metal surfaces.

Conclusions We demonstrated arrays of super-hydrophobic gold nanoparticles for metal enhanced fluorescence. Dividing the fabrication process of the chip into two separate stages permits to realize devices in which the size and spacing of the (i) silicon pillars and the (ii) gold particles are controlled separately at the micro to nano level in a three-dimensional architecture. The described device takes advantage of a hierarchical structure in which super-hydrophobic effects and metal enhanced fluorescence of gold nanoparticles arrays combine to yield increased fluorescence efficiency in comparison to untreated planar substrates. This, in turn, enables to operate site specific measurements of biological samples with high sensitivity and low detection ranges. The described technology may be principally used in in protein microarrays, enabling

multiplexed protein assays with detection limits as low as few femto-molar and high dynamic range, for the early detection of cancer biomarkers or other proteins.

Acknowledgments

This work has been partially funded from the Italian Minister of Health (Project n. GR-2010-2320665) and by UE, MIUR and Ministero dello Sviluppo Economico (project ITEM (Infrastruttura per Tecnologie BioMEMS di Sensing Avanzato per Monitoraggio e Diagnostica Ambientale e Alimentare) PONa3_00077).

Figure Captions

Figure 1 Super-Hydrophobic silicon micro-pillars are arranged in in a hexagonal lattice in the plane over extended regions of the substrate (**a**); high magnification SEM micro-graphs of the upper surface of the pillars reveal the morphology of the gold nanoparticles clusters, where the average diameter of the particles is 60 nm (**b, c**). AFM profile of the gold nanoparticles clusters was acquired (**d**) and analysed to extract the information content of the image over different scales (**e**), from this, the fractal dimension of the structures is derived as $D_f = 2.4$, that is strictly larger than the Euclidean dimension of surface $D = 2$.

Figure 2 simulations of the electromagnetic (EM) field around Au nanoparticles clusters were performed using a finite element method (FEM). Nanoparticles are represented as partially overlapping spheres (**a**), where the diameter of the spheres ranges from 50 to 60 nm. EM amplifications and charge density reach a maximum at the particle-particle interfaces (**b, c**). For this configuration, the maximum EM increment is $Q \sim 15$, and thus the MEF amplification is $Q^2 \sim 225$.

Figure 3 the devices were demonstrated in the analysis of fluorescent $GBP - FITC$ gold binding peptide. The fluorescence signal emitted by not treated cluster gold surfaces (**a**), compared to the high signal measured on super-hydrophobic clusters of gold nanoparticles adsorbed by GBP-FITC, in the plane (**b**) and in the longitudinal direction (**c**). MEF on the metal nanostructures is confirmed by fluorescence lifetime images (FLIM), which reveal the extent of fluorescence

lifetime on the untreated bi-dimensional metal nanostructures (**d**) in comparison to the fluorescence lifetime measured on functionalized super-hydrophobic gold nanoparticles clusters (**e**).

Table 1 Fluorescence lifetime imaging (FLIM) parameters measured on non-functionalized planar gold substrates compared to those measured on functionalized super-hydrophobic clusters of gold nanoparticles.

References

[1] S. Glotzer, Nanotechnology: Shape Matters, Nature 481 (2012) 450-452.

[2] G. Das, E. Battista, G. Manzo, F. Causa, P. Netti, E. Di Fabrizio, Large-scale plasmonic nanocones array for spectroscopy detection, ACS Applied Materials and Interfaces 7(42) (2015) 23597-23604.

[3] W. Deng, F. Xie, H.T.M.C.M. Baltarac, E.M. Goldys, Metal-enhanced fluorescence in the life sciences: here, now and beyond, Physical Chemistry Chemical Physics 15(38) (2013) 15695-15708.

[4] K. Ray, J.R. Lakowicz, Metal-Enhanced Fluorescence Lifetime Imaging and Spectroscopy on a Modified SERS Substrate, Journal of Physical Chemistry C 117 (2013) 15790−1579.

[5] S.M. Tabakman, L. Lau, J.T. Robinson, J. Price, S.P. Sherlock, H. Wang, B. Zhang, Z. Chen, S. Tangsombatvisit, J.A. Jarrell, P.J. Utz, H. Dai, Plasmonic substrates for multiplexed protein microarrays with femtomolar sensitivity and broad dynamic range, Nature Communications 2(466) (2011) 1-9.

[6] M.L. Coluccio, F. Gentile, M. Francardi, G. Perozziello, N. Malara, P. Candeloro, E. Di Fabrizio, Electroless Deposition and Nanolithography Can Control the Formation of Materials at the Nano-Scale for Plasmonic Applications, Sensors 14(4) (2014) 6056-6083.

[7] F. Gentile, M. Coluccio, A. Toma, E. Rondanina, M. Leoncini, F. De Angelis, G. Das, C. Dorigoni, P. Candeloro, E. Di Fabrizio, Electroless deposition dynamics of silver nanoparticles

clusters: A diffusion limited aggregation (DLA) approach Microelectronic Engineering 98 (2012) 359-362.

[8] F. Gentile, M.L. Coluccio, R.P. Zaccaria, M. Francardi, G. Cojoc, G. Perozziello, R. Raimondo, P. Candeloroa, E.D. Fabrizio, Selective on site separation and detection of molecules in diluted solutions with superhydrophobic clusters of plasmonic nanoparticles, Nanoscale 6 (2014) 8208-8225.

[9] F. Gentile, G. Das, M. Coluccio, F. Mecarini, A. Accardo, L. Tirinato, R. Tallerico, G. Cojoc, C. Liberale, P. Candeloro, P. Decuzzi, F. De Angelis, E. Di Fabrizio, Ultra low concentrated molecular detection using super hydrophobic surface based biophotonic devices, Microelectronic Engineering 87 (2010) 798-801.

[10] F. Gentile, M. Coluccio, N. Coppedè, F. Mecarini, G. Das, C. Liberale, L. Tirinato, M. Leoncini, G. Perozziello, P. Candeloro, F. De Angelis, E. Di Fabrizio, Superhydrophobic Surfaces as Smart Platforms for the Analysis of Diluted Biological Solutions, ACS Applied Materials and Interfaces 4(6) (2012) 3213–3224.

[11] T. Limongi, F. Cesca, F. Gentile, R. Marotta, R. Ruffilli, A. Barberis, M.D. Maschio, E.M. Petrini, S. Santoriello, F. Benfenati, E. Di Fabrizio, Nanostructured Superhydrophobic Substrates Trigger the Development of 3D Neuronal Networks, Small 9(3) (2013) 402–412.

[12] F. Gentile, E. Battista, A. Accardo, M. Coluccio, M. Asande, G. Perozziello, G. Das, C. Liberale, F. De Angelis, P. Candeloro, P. Decuzzi, E. Di Fabrizio, Fractal Structure Can Explain the Increased Hydrophobicity of NanoPorous Silicon Films, Microelectronic Engineering 88 (2011) 2537-2540.

[13] F. Gentile, L. Tirinato, E. Battista, F. Causa, C. Liberale, E. Di Fabrizio, P. Decuzzi, Cells preferentially grow on rough substrates, Biomaterials 31(28) (2010) 7205-12.

[14] F. Gentile, R. Medda, L. Cheng, E. Battista, P.E. Scopelliti, P. Milani, E.A. Cavalcanti-Adam, P. Decuzzi, Selective modulation of cell response on engineered fractal silicon substrates, Sci. Rep. 3 (2013).

[15] F. Causa, R. Della Moglie, E. Iaccino, S. Mimmi, D. Marasco, P.L. Scognamiglio, E. Battista, C. Palmieri, C. Cosenza, L. Sanguigno, I. Quinto, G. Scala, P.A. Netti, Evolutionary screening and adsorption behavior of engineered M13 bacteriophage and derived dodecapeptide for selective decoration of gold interfaces, Journal of Colloid and Interface Science 389(1) (2013) 220-229.

[16] C. Cosenza, V. Lettera, F. Causa, P. Scognamiglio, E. Battista, P. Netti, Cell mechanosensory recognizes ligand compliance at biomaterial interface, Biomaterials 76 (2015) 282-291.

[17] A.M. Cusano, F. Causa, R.D. Moglie, N. Falco, P.L. Scognamiglio, A. Aliberti, R. Vecchione, E. Battista, D. Marasco, M. Savarese, U. Raucci, N. Rega, P. Netti, Integration of binding peptide selection and multifunctional particles as tool-box for capture of soluble proteins in serum, Journal of the Royal Society: Interface 11(99) (2014) 20140718:1-11.

[18] A.D. Rakić, A.B. Djurišić, J.M. Elazar, M.L. Majewski, Optical properties of metallic films for vertical-cavity optoelectronic devices, Applied Optics 37(22) (1998) 5271-5283.

[19] A.C. Manikas, A. Aliberti, F. Causa, E. Battista, P.A. Netti, Thermoresponsive PNIPAAm hydrogel scaffolds with encapsulated AuNPs show high analyte-trapping ability and tailored plasmonic properties for high sensing efficiency, J. Mater. Chem. B 3(1) (2015) 53-58.

	τ1 (ns)	*fractional*	τ2 (ns)	*fractional*	τ average (ns)
Au reflection	0.078	0.87	0.713	0.13	0.16
GBP-FITC on Gold	0.089	0.59	1.83	0.41	0.8

Table 1

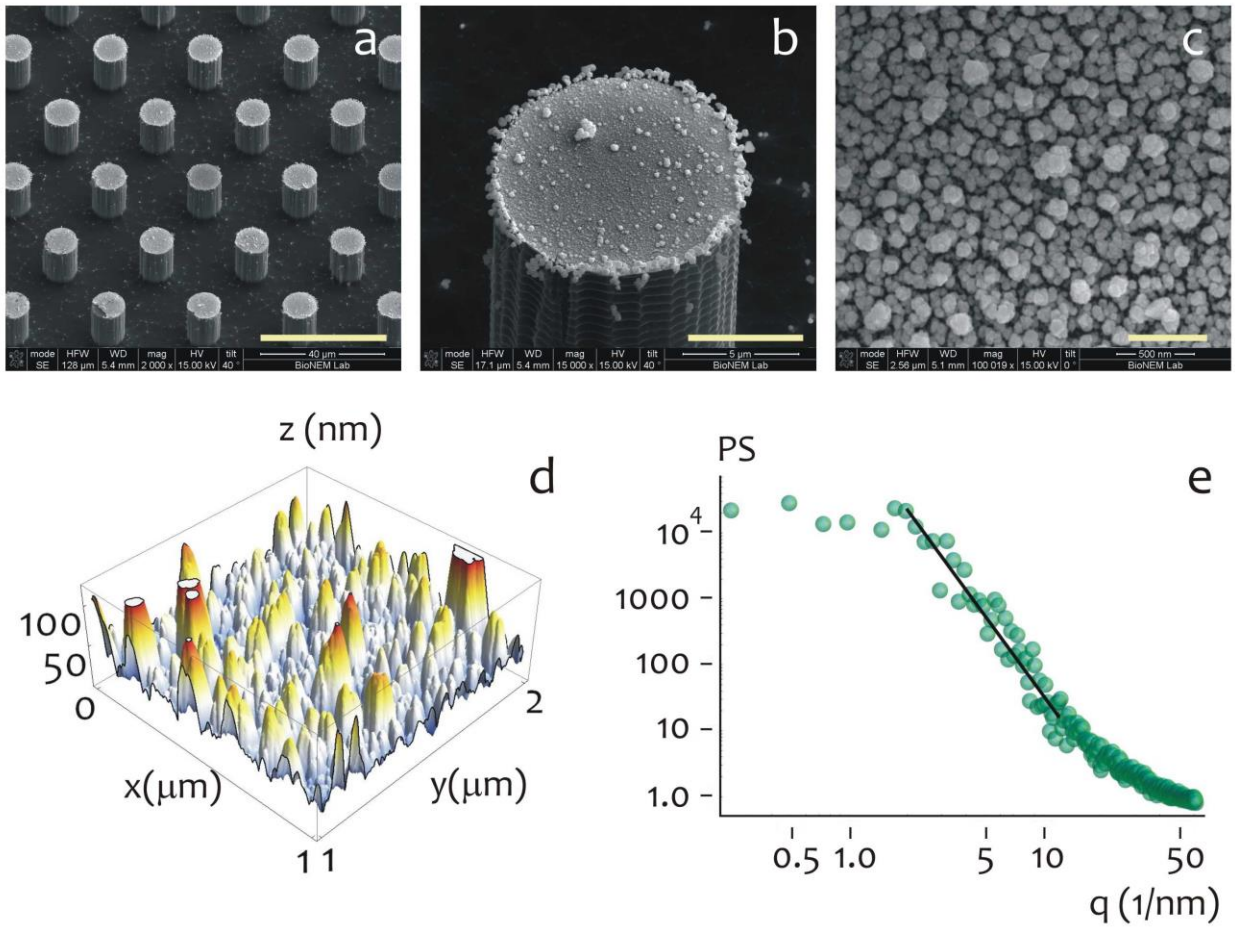

Fig. 1

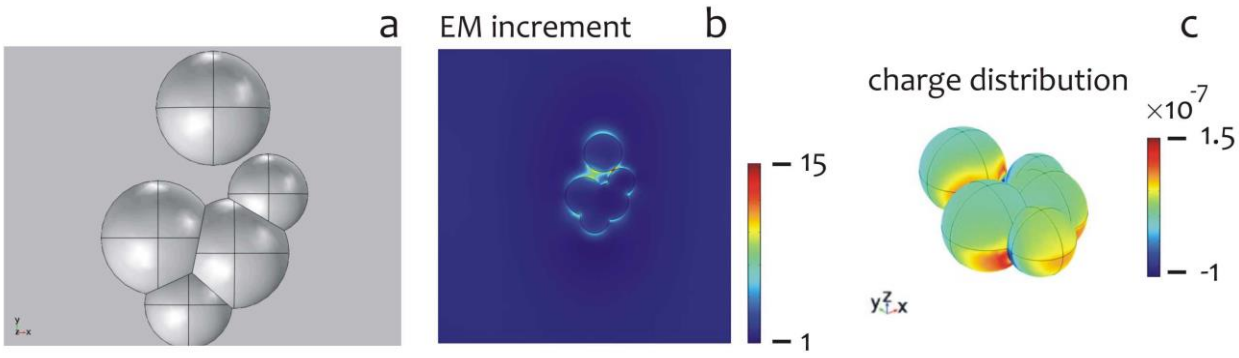

Fig. 2

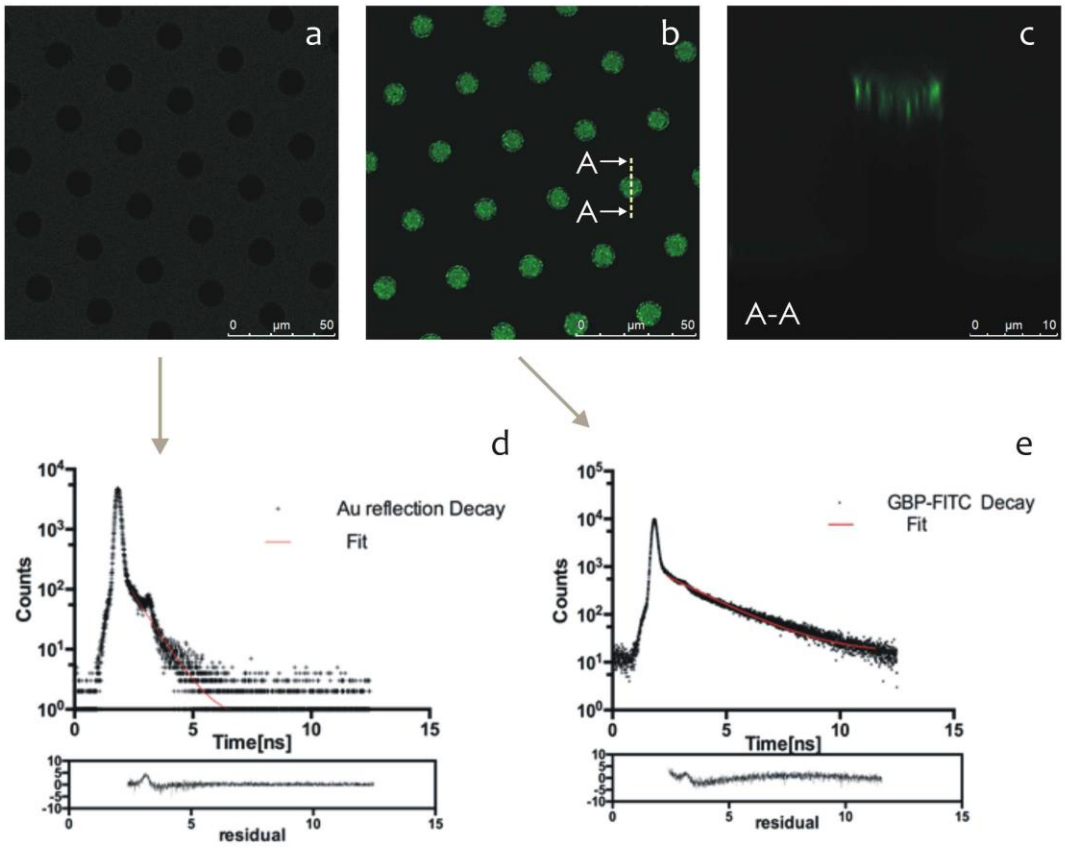

Fig. 3

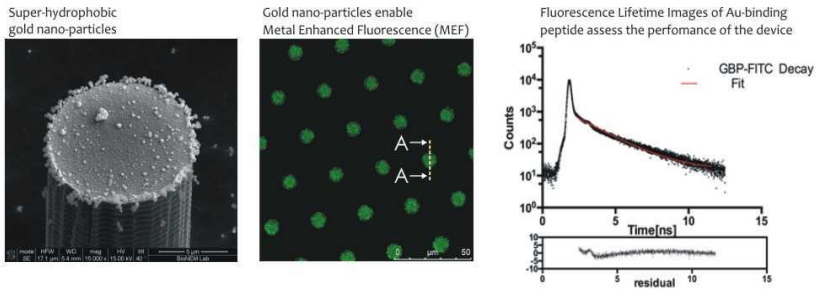

Graphical abstract

Highlights

Arrays of super-hydrophobic Si μPillars with gold nanoparticles on top manipulate and concentrate biological solutions

Gold-binding peptides respresent an alternative method for selective functionalization of gold nanoparticle surfaces

Gold nanoparticles enable metal enhanced fluorescence (MEF) effects that amplify fluorescence signal by orders of magnitude

We demonstrated theoretical and experimental analyses of fluorescein derived gold-binding peptides